

TADA: Temporal Adversarial Data Augmentation for Time Series Data

Byeong Tak Lee*, Joon-myung Kwon, and Yong-Yeon Jo[†]

AI Group

Medical AI Co., Ltd.

Seoul, Republic of Korea

{bytaklee, yy.jo}@medicalai.com

Abstract

Domain generalization involves training machine learning models to perform robustly on unseen samples from out-of-distribution datasets. Adversarial Data Augmentation (ADA) is a commonly used approach that enhances model adaptability by incorporating synthetic samples, designed to simulate potential unseen samples. While ADA effectively addresses amplitude-related distribution shifts, it falls short in managing temporal shifts, which are essential for time series data. To address this limitation, we propose the Temporal Adversarial Data Augmentation for time series Data (TADA), which incorporates a time warping technique specifically targeting temporal shifts. Recognizing the challenge of non-differentiability in traditional time warping, we make it differentiable by leveraging phase shifts in the frequency domain. Our evaluations across diverse domains demonstrate that TADA significantly outperforms existing ADA variants, enhancing model performance across time series datasets with varied distributions.

1 Introduction

Most machine learning models are developed on the assumption that their training data reliably represents the broader population. Unfortunately, this assumption is often incorrect. The distribution of real-world data often deviates from that of the training dataset, and such discrepancies lead to performance degradation [1–5]. An adversarial data augmentation (ADA) is one of the approaches that addresses distribution shift problem by solving worst-case scenarios around the original distribution [1, 2]. By training the model with adversarial synthetic samples, which are made extremely difficult for the model to classify, we can ensure that the model performs reliably under less challenging conditions, such as distribution shift.

Time series data can be depicted on a 2D graph, with the amplitude axis representing magnitude of data points and the temporal axis indicating the sequence and timing of these points. While ADA effectively simulates samples that reflect distribution shifts related to amplitude axis, it is limited in generating samples that account for distribution shifts along the temporal axis [6, 7]. Since distribution shifts in time series data are associated with both axes, it is crucial to develop methods that also account for changes along the temporal axis.

To address the challenge of distribution shift along the time axis, we propose Temporal Adversarial Data Augmentation (TADA) for time series data. This method integrates a time warping technique with the ADA process [8, 9]. A significant challenge in directly applying time warping within ADA is the non-differentiable nature of index mapping, which disrupts gradient computation with respect

*First Author.

[†]Corresponding Author.

to the input loss. To overcome this, we introduce parameterized phase shifts in the frequency domain. This approach enables distinct, differentiable phase shifts for individual segments of the time series data, effectively approximating time warping in the time domain. Our method thus facilitates a differentiable form of time warping, enhancing the robustness of model training against temporal variations.

To evaluate the effectiveness of our method for distribution shifts, we used different types of time series datasets, such as electrocardiogram (ECG), electroencephalogram (EEG), and human activity recording (HAR) [10, 11]. Each dataset consists of multiple distinct subgroups, each distinguished by different distributions. We conducted experiments on a single source domain generalization scenario, where models were trained on one subgroup and then evaluated on the remaining subgroups [12].

The results clearly demonstrate that the TADA enhances model performance across target domain with distribution different from those in the source domain. TADA’s straightforward implementation, which involves inserting a proposed time-warping function between the input and the encoder, ensures it is compatible with other variants of ADA. Our experiments reveal that incorporating the proposed time-warping function boosts the performance of existing ADA variants. Finally, we evaluated whether TADA can simulate real-world distribution shifts. Our observations confirm that TADA effectively simulates real-world distributions in latent space, emphasizing its value in addressing the distribution shifts problems in time series data.

The contributions of this paper are as follows: (1) We identify a significant issue with the existing ADA approaches in time series data, particularly their inability to effectively handle temporal dynamics and distribution changes. (2) We propose a novel ADA specifically designed to perturb data along the temporal axis, thus enhancing the robustness of models against time-related variations in data distribution. (3) We demonstrate that our proposed method is highly effective in extensive experiments on the single-source domain generalization framework.

2 Related works

Domain Generalization. The distribution shift between source domain and unseen target domain often degrades [13–15]. Domain generalization emerges to address these problems. The goal of domain generalization is to train models to effectively generalize across multiple unseen target domain [16, 3, 17, 18].

Depending on the coverage of the source domain, domain generalization is categorized into single-source and multiple-source domain generalization [12, 18]. For single-source domain generalization, the objective is to generalize the model when only a single domain is available for training. Since identifying domain-specific characteristics within the training dataset is impossible, single-domain generalization rely on generating fictitious distribution that simulate unseen domains. This includes data augmentation-based methods [1–3, 12]. For the multiple-source domain generalization, the objective is to learn invariant features across multiple domains that are not affected by domain shift in the source domain. This is based on the idea that the unchanging characteristics will also remain consistent in the unseen target domain, and domain alignment is a widely adopted approach in multiple-source domain generalization [4, 5, 19].

Adversarial Data Augmentation. Adversarial Data Augmentation (ADA) enhances a model’s ability to generalize across other domain or unseen distributions. This method tackle the worst-case problem as detailed in Equation 1 [1]. By employing ADA, the model achieves robust performance even when the distribution P differs markedly from the initial domain P_0 , effectively handling scenarios of domain shift.

$$\min_{\theta \in \Theta} \{ \sup_P \{ \mathbb{E}[\mathcal{L}(\theta; X, Y)] - \gamma D_\theta(P, P_0) \} \}, \quad (1)$$

where X and Y denote a sample and its corresponding label, respectively, and γ is a penalty parameter.

In practical, an iterative training procedure that alternates between the maximization phase and the minimization phase is conducted. For the maximization phase, data points are generated from fictitious distribution P , which is constrained to deviate within a distance P from the source distribution P_0 . On the other hand, for the minimization phase, the network θ is updated to minimize loss on the data sampled from both P and P_0 .

There are several studies presenting variations of ADA: Zhao et al. [2] advance adversarial domain augmentation by maximizing the entropy of feature representation, which leads to generated samples covering a broad spectrum of potential distribution shifts. On the other hand, Qiao et al. [12] introduce the meta-learning scheme and the Wasserstein Auto-Encoder to relax the worst-case constraint.

Time Warping. Time warping is a technique used to align sequences of time series data that may vary in time or speed [8, 9]. It is commonly employed as a data augmentation method to modify the temporal characteristics of the data. Intuitively, time warping involves manipulating the temporal scaling between points in a time series, either by stretching or compressing the timing of the sequence, while preserving its overall trajectory. To implement time warping effectively, a warping path is crucial; it represents a sequence of points that map the indices from one time series to the indices of another.

The warping path must satisfy the following conditions [20]:

- **Maintaining Monotonicity:** The ordering of points in the sequence is kept monotonic.
- **Boundary Alignment:** The sequences are aligned at both the starting and ending points.
- **Warping Distance Constraint:** The index shift caused by index mapping is limited, ensuring that the difference between corresponding indices does not exceed a predefined width.

3 Methodology

3.1 Problem Formulation

ADA consists of maximization phase, which focuses on data generation, and a minimization phase, which involves updating the model. We will redesign the maximization phase of ADA to generate samples with distribution shift in temporal axis. Equation 2 represents the objective of the maximization phase from Equation 1.

$$X^k \in \arg \max_X \{ \mathcal{L}(\theta; (X^{k-1}, Y)) - \gamma c_\theta((X^{k-1}, Y), (X^0, Y)) \}, \quad (2)$$

where k refers the number of iteration for adversarial update, X^0 and X^k are original samples and adversarial perturbed samples at the iteration k , respectively. γ is a penalty parameter, and c_θ is a distance measure.

The maximization phase can simply be understood as the addition of adversarial noise to the input, expressed as $\hat{x} = x + \Phi$, where Φ represents the noise added. This process can be thought as passing the input sample through a function F , which is parameterized by Φ : $\hat{x} = F(x; \Phi) = x + \Phi$. Now, we update Φ instead of X iteratively as following Equation 3:

$$\Phi^k \in \arg \max_\Phi \{ \mathcal{L}(\theta; (F(X; \Phi^{k-1}), Y)) - \gamma c_\theta((F(X; \Phi^{k-1}), Y), (X, Y)) \} \quad (3)$$

Our objective is to design a function F that alters the temporal characteristic of the time series data X without affecting its amplitude. To achieve this, we can think of incorporating the time warping in the function F to transform the sequence according to a warping path. However, the time warping is non-differentiable since it uses the index mapping. This makes iterative updating of Φ infeasible.

3.2 Differentiable Time Warping

To address this issue, we propose a new time warping function F that is equivalent to traditional time warping but differentiable. Leveraging the duality of time shift in the time domain, which is non-differentiable, and a phase shift in the frequency domain, which is differentiable, we introduce differentiable time warping.

We begin with the mathematical formulation of time warping. Time warping involves a specific warping path, which maps the index of original sequence to transformed sequence. Applying time warping to a sequence of the time series data $X = \{x_1, x_2, \dots, x_n\}$ transforms it into the transformed sequence $X' = \{x_{1+\delta_1}, x_{2+\delta_2}, \dots, x_{n+\delta_n}\}$, where δ indicates the distance that an index is moved from its current position (e.g., time shift), and $\Delta = \{\delta_1, \delta_2, \dots, \delta_n\}$ means the warping path.

The time warping can be derived from an alternative perspective. We first consider to divide the sequence of original time series X into overlapping segments, each of which s_i is represented to $\{x_{i-m}, \dots, x_i, \dots, x_{i+m}\}$. Once a segment s_i is shifted by δ_i , all its points move the same distance, resulting in $x_{i-m+\delta_i}, \dots, x_{i+\delta_i}, \dots, x_{i+m+\delta_i}$. After shifting, we only extract the central part of each segment $x_{i+\delta_i}$, and aggregate them. Finally, we can get the transformed sequence $X' = \{x_{1+\delta_1}, x_{2+\delta_2}, \dots, x_{n+\delta_n}\}$, which is identical to that obtained through time warping.

Here, time shifts for each segment s can be substituted with a phase shift in the frequency domain, leveraging the fact that a time shift in the time domain is the dual of a phase shift in the frequency domain. It is crucial to note that phase shifts in the frequency domain involve additive operations, which are inherently differentiable.

Combining all these together, then we have the following Proposition 1.

Proposition 1. *Applying time warping to a sequence, X' , is equivalent to applying phase shift $\Delta\Phi_j$ to the frequency domain components of a sub-sequence S_i , defined as a contiguous segment of the original sequence.*

$$\text{TimeWarping}(X) = \{f'^{-1}(g(f(s_1), \Phi_1)), \dots, f'^{-1}(g(f(s_n), \Phi_n))\} \quad (4)$$

Proposition 1 presents three steps.

1. The function f splits the time series data X into multiple segments $s \in S$ and transforms these segments into their corresponding outputs in the frequency domain.
2. The function g then applies the phase shift Φ to the frequency domain components $f(s)$, resulting in a phase shift. In this context, the parameter Φ serves as the warping path.
3. Finally, the function f'^{-1} transforms the phase-shifted components back into segments $s \in S$ in the time domain. The time-shifted time series data X' is obtained by aggregating these segments S .

3.2.1 Function f : Transformation to frequency domain

We first split time series data X into overlapping segments S because applying a phase shift to a segment results in the same distance shift across all its points. Thus, A point x_i in the time series data X can belong to multiple segments, depending on the window size and the degree of overlap. The number of segments that a single point x_i belongs to can vary based on how the segments are defined and the chosen window size. The function f converts these segments into the frequency domain. In practice, function f is typically implemented using the Short-Time Fourier Transform (STFT) as the following Equation 5:

$$f(s)[m, k] = \sum_{n=0}^{N-1} x[n]w[n-m] \cdot e^{-j2\pi kn/N} = \chi[m, k], \quad (5)$$

where k is the frequency bin index, m is the frame index, N is the number of frequency bins, and χ is a output corresponding to segment s in the frequency domain.

Here, the window function w is defined as follows:

$$w[n-m] = \begin{cases} 1, & \text{if } |n-m| < M, \\ 0, & \text{otherwise,} \end{cases} \quad (6)$$

where M is the maximum window length.

3.2.2 Function g : Time warping in frequency domain

To apply the time warping in frequency domain, we perturb the temporal characteristics of a output χ_i for the segment s_i by adding the noise that induces a corresponding phase shift Φ_i , resulting in $g(f(s), \Phi) = f(s) + \Phi \cdot \omega$. A Φ is interpreted as the warping path.

The warping path must fulfill several conditions [20]: (1) it must be monotonic, ensuring that the sequence progresses in a single direction without reversals; (2) it must align with the boundaries, meaning the start and end indices of the path should coincide the start and end of the sequences being aligned; and (3) it must adhere to a warping distance constraint, which limits the extent of the warping. To ensure these conditions, we impose several constraints on Φ using the function g . With constraints, Φ is redefined as $\Phi = (g_3 \cdot g_2 \cdot g_1)(\phi)$, with ϕ denoting the perturbation parameters.

Maintaining Monotonicity. The monotonicity constraint ensures that the original indices in the warping path consistently map forwarding indices to be transformed, never reversing direction. This means that if a point in the original sequence a_i is aligned with a point in a transformed sequence b_j , then a_{i+1} can only be aligned with b_j or its subsequent points $b_{j+k}, k \geq 0$. Fulfilling the requirement of monotonicity means that the difference between consecutive element of the warping path must be non-negative. This can be expressed by $\phi_i \geq 0$. To ensure that each element of the warping path remains non-negative, we subtract the minimum value found in the warping path element from each element as follows:

$$g_1(\phi_i) = \sum_{i=1}^{\tau} \phi_i - \min(\phi) \quad (7)$$

Boundary Alignment. To ensure indices of elements in the transformed sequence aligned in the boundary (e.g., starting and ending indices) of the original sequence, we first normalize ϕ_i and then scale the normalized path to match the length of original signal, resulting in the warping path. On this warping path, each element is subtracted by the order of index, which gives the difference between the original index and the corresponding index in the shifted sequence. This is represented as below:

$$g_2(\phi_i) = \frac{\max(\phi) - \phi_i}{\max(\phi) - \min(\phi)} \cdot N - i, \quad (8)$$

where N denotes the total number of the segment (i.e. signal length).

Warping Distance Constraint. To prevent the transformed sequence from deviating excessively from the original, we impose a constraint on the level of deviation. As described in Equation 9, we define ϕ_{\max} as a hyperparameter for the upper limit for the maximum allowable deviation between the indices of the original and the transformed sequences. For example, if ϕ_{\max} is set to 10, the index in the transformed sequence cannot deviate more than 10 indices far from its corresponding index in the original sequence. To preserve the fidelity of the transformation process, it is crucial to choose ϕ_{\max} to be shorter than the window size used when transforming the signal to the frequency domain. This approach ensures that the deviation stays within acceptable boundaries.

$$g_3(\phi_i) = \phi_i \cdot \min\left(\frac{\phi_{\max}}{\|\phi\|_{\infty}}, 1\right) \quad (9)$$

In the equation above, if the infinity norm of the elements of ϕ (i.e., $\|\phi\|_{\infty}$) is greater ϕ_{\max} , ϕ is rescaled to ensure that all element absolute values remain below ϕ_{\max} .

3.2.3 Function f'^{-1} : Reconstruction to time domain

After perturbing the signal in the frequency domain, we use Inverse STFT (ISTFT) to reconstruct the segment s in the time domain. ISTFT converts a frequency-domain component χ into its corresponding segment s as Equation 10.

$$s[n] = \frac{1}{\sum_{n=0}^{N-1} w'^2[n]} \sum_m \sum_{k=0}^{N-1} \chi[m, k] w'[n - m] e^{j2\pi kn/N}, \quad (10)$$

In Section 3.2.1, we described how the time series data X is divided into overlapping segments S to facilitate the application of distinct phase shifts across all segments. This process leads to interference among the time-shifted segments when aggregating them back into the time series data X . Instead of averaging the overlapping windows in the function f as described in Equation 5, we extract the central value from each transformed segment using a specific window function w' in the inverse function f'^{-1} .

$$w'[n - m] = \begin{cases} 1, & n = m \\ 0, & \text{otherwise} \end{cases} \quad (11)$$

3.3 Training Procedure

We describe the full procedure on Algorithm 1. Our proposed algorithm incorporates adversarial data augmentation to improve model robustness through an iterative training process, which the

overall training scheme is identical to ADA [1]. Initially, the algorithm accepts an original dataset D_0 , initialized weights θ_0 , and a perturbation parameter ϕ_0 . The model weights are set to θ_0 at the beginning (Line 3).

During each of the K epochs, the algorithm first performs a series of mini-batch updates (lines 4-7). For each mini-batch t from 1 to T_{min} , a data pair (X_t, Y_t) is sampled uniformly from D_{k-1} (line 6). The model weights θ are then updated by gradient descent (line 7).

Following the updates, the sampled dataset $\{X_i, Y_i\}_{i=1}^n$ from D_{k-1} undergoes an adversarial perturbation phase (lines 9-17). Samples is perturbed over T_{max} iterations (lines 12-14). The perturbation parameter (i.e., warping path) ϕ_i^k is initialized and optimized the adversarial loss (lines 13). Each perturbed samples $(F(X_i, \phi_i^k), Y_i)$ is then appended to expand the dataset D_k (line 15).

After completing all epochs for the maximization phase, the minimization phase is performed on the augmented dataset D_K (lines 18-20). For T epochs, the model weight θ is updated by samples (X, Y) (line 20).

Algorithm 1 Training Procedure using Temporal Adversarial Data Augmentation

```

1: Input: original dataset  $D_0 = \{X_i, Y_i\}_{i=1}^n$  and initialized weights  $\theta_0$ , perturbation parameter  $\phi_0$ 
2: Output: learned weights  $\theta$ 
3: Initialize:  $\theta \leftarrow \theta_0$ 
4: for  $k = 1, \dots, K$  do
5:   for  $t = 1, \dots, T_{min}$  do
6:     Sample  $(X_t, Y_t)$  uniformly from dataset  $D_{k-1}$ 
7:      $\theta \leftarrow \theta - \alpha \nabla_{\theta} \mathcal{L}(\theta; X_t, Y_t)$ 
8:   end for
9:   Sample  $\{X_i, Y_i\}_{i=1}^n$  from the dataset  $D_{k-1}$ 
10:  for  $i = 1, \dots, n$  do
11:    Initialize:  $\phi_i^k \leftarrow \phi_0$ 
12:    for  $t = 1, \dots, T_{max}$  do
13:       $\phi_i^k \leftarrow \phi_i^k + \eta \nabla_{\phi} \{\mathcal{L}(\theta; (F(X_i, \phi_i^k), Y_i)) - \gamma c_{\phi}((F(X_i, \phi_i^k), Y_i), (X_i, Y_i))\}$ 
14:    end for
15:    Expand dataset  $D_k$  by appending  $(F(X_i, \phi_i^k), Y_i)$ 
16:  end for
17: end for
18: for  $t = 1, \dots, T$  do
19:   Sample  $(X, Y)$  uniformly from dataset  $D_K$ 
20:    $\theta \leftarrow \theta - \alpha \nabla_{\theta} \mathcal{L}(\theta; (X, Y))$ 
21: end for

```

4 Experiments

In this section, we benchmark our proposed method against leading techniques within the single domain generalization framework, which involves training models on data from one domain and deploying them in another. Additionally, we perform ablation studies to assess the effects of integrating our method with other approaches. Lastly, by analyzing the representations extracted from models trained using our methodology, we confirm that our method effectively simulates a valid distribution shift.

4.1 Experimental Setup

Datasets. Datasets used in our experiments consist of multiple sub-datasets. The sub-datasets were sourced from various regions or collected using different devices, leading inherent distribution shifts among them. This diversity among sub-dataset allows a comprehensive evaluation of methods robustness across varied data characteristics.

Physionet Challenge 2021 (Physionet) dataset [10] is a public dataset for electrocardiogram (ECG) research, aimed at diagnosing a wide range of cardiac abnormalities. It consists of seven sub-datasets. Each dataset presents differences in demographic profiles. Among them, five datasets containing over 1,000 ECGs were selected for our experiment: PTB-XL [21], Chapman-Shaoxing [22], Ningbo [23], G12EC, and CPSC2018 [24]. The datasets involve multi-label classification of 26

arrhythmia classes; however, only seven classes are common across all datasets. Thus, we set a target task to the multi-label classification for these seven labels.

Woods-PCL (PCL) dataset [11] is a electroencephalogram (EEG) collection aimed at distinguishing imagined hand movement. It was collected from three distinct medical centers, each with different collection procedures from different research group. These differences during data gathering can causes distribution shifts, affecting clinical model failures [25].

Woods-HHAR (HHAR) dataset [11] is a signal dataset that records human activity recognition from smart devices equipped with three-axis accelerometers and gyroscopes. The objective of the task is classify one of six human activity, including sitting, walking, and running. Data was collected from five different types of devices, each processed using distinct hardware features and signal processing techniques. These variations can lead to distribution shift between the different smart devices.

Implementation details. We note that the objective of this study is not improving the performance of the network architecture. Thus, we adopted ResNet18 as the backbone network. For all experiments, we used the Adam optimizer [26] and the cyclic learning rate scheduler [27] with a 10-epoch period. The batch size was set to 512. In TADA parameters, we set T_{max} to 10, T_{min} to 10, and K to 2. The dropout rate is randomly chosen from 0 to 0.3 in increments of 0.05. For both ADA and TADA, γ was randomly selected in $\{0.1, 1, 10\}$. The parameter η was selected from $\{100, 200, 500\}$ for ADA and fixed as 1 for TADA. The window size M for STFT in TADA was set to 10.

For the Physionet dataset, the learning rate was randomly selected from the range $[10^{-5}, 10^{-3}]$, and the weight decay was chosen from $[10^{-5}, 10^{-3}]$. For the PCL and HHAR datasets, the learning rate is randomly selected from the range $[10^{-4}, 10^{-2}]$, and the weight decay is chosen from $[10^{-4}, 10^{-2}]$, respectively.

As a scheduler for the hyperparameter tuning, we used the asynchronous successive halving algorithm, set with a grace period 10 and a reduction factor of 2 [28]. The entire training workflow was implemented with the Ray framework [29].

Comparison methods. We compared the proposed method with seven approaches: (1) Empirical Risk Minimization (ERM) is a fundamental training principle widely used in machine learning. This is used as a standard baseline method. (2) Mixup [30] uses convex combinations of pairs of samples and their labels as inputs to train a network. (3) RandConv [31] uses multi-scale random convolutions as a data augmentation method to generate samples with randomized local textures while preserving global shapes. (4) ADA [1] is an adversarial training to generate new training examples by introducing perturbations designed to maximize prediction error of the model. (5) ME-ADA [2] is an extension of ADA by adopting a maximum-entropy criterion. (6) M-ADA [32] is an extension of ADA that relax the worst-case constraint to encourage large domain transportation. All comparison methods only focus on applying perturbation with respect to the amplitude of the signal without temporal shift.

Evaluation. To evaluate the single domain generalization framework, we trained the model on each sub-dataset and then evaluated it on the remaining sub-datasets, using the average performance across these sub-datasets. For each sub-dataset, we measured the macro F1 score as the performance metric to ensure a balanced assessment across classes. To avoid distortion in the results, hyperparameters were tuned for each training session by exploring 30 different combinations.

4.2 Performance Evaluation on Datasets with Different Domains

In the following tables, scores in boldface indicate the best performance, and underlined scores represent the second best. A column includes ADA+TADA meaning a combination of ADA and TADA.

Physionet dataset. Table 1 shows the average F1 scores on the Physionet dataset. For the PTBXL dataset, methods including the proposed one like TADA and ADA+TADA are the most effective. The G12EC dataset shows a close performance among several methods, with TADA leading slightly. The CPSC2018 dataset, which generally presents lower scores, finds Mixup to be the most effective method. For the Chapman dataset, the combination of ADA and TADA acheive the best. Lastly, the Ningbo dataset shows that ADA+TADA outperforms other methods. Overall, in the ECG domain,

the average scores present ADA+TADA as the best method. We have confirmed that applying TADA or RandConv enhances the model performance.

Table 1: F1 score on the Physionet dataset

Dataset	ERM	Mixup	RandConv	ADA	ME-ADA	M-ADA	TADA	ADA+TADA
PTBXL	0.4943	0.4918	0.4863	0.4681	0.4835	0.4769	0.4957	0.4957
G12EC	0.4628	<u>0.4723</u>	0.4609	0.4631	0.4578	0.4694	0.4745	0.4721
CPSC2018	0.3820	0.3971	0.3938	0.3749	0.3752	0.3719	0.3565	0.3737
Chapman	0.4561	0.4554	<u>0.4702</u>	0.4561	0.4692	0.4649	0.4588	0.4737
Ningbo	0.5174	0.5321	<u>0.5349</u>	0.5149	0.5276	0.5278	0.5272	0.5389
Average	0.4625	<u>0.4697</u>	0.4692	0.4554	0.4627	0.4622	0.4625	0.4708

PCL dataset. Table 2 presents the average F1 scores on the PCL dataset. In Dataset1, RandConv emerges as the best method, with TADA following as the second one. Dataset2 and Dataset3 show that ADA+TADA achieve the best performance, respectively. Overall, ADA+TADA showed the best performance on EEG datasets, and methods that included TADA consistently led to high performance.

Table 2: F1 score on the PCL dataset

Method	ERM	Mixup	RandConv	ADA	ME-ADA	M-ADA	TADA	ADA+TADA
Dataset1	0.6367	0.6304	0.6877	0.6368	0.6265	0.6352	<u>0.6426</u>	0.6203
Dataset2	0.6080	0.5940	0.5875	<u>0.6158</u>	0.5950	0.6053	0.5994	0.6161
Dataset3	0.5898	<u>0.6001</u>	0.5732	0.5935	0.5895	0.5931	0.5923	0.6277
Average	0.6115	0.6082	<u>0.6161</u>	0.6154	0.6036	0.6112	0.6114	0.6214

HHAR dataset. Table 3 shows the experimental result on HHAR dataset. We observed that the best methods are distributed across the different datasets. In the overall results, we noticed that when TADA was used independently, its performance significantly dropped, contrary to trends seen in other datasets in ECG and EEG domains. This suggests that the HHAR dataset may not particularly account for temporal features. Fortunately, the combination of TADA and ADA ultimately resulted in the best performance.

Table 3: F1 score on the HHAR dataset

Dataset	ERM	Mixup	RandConv	ADA	ME-ADA	M-ADA	TADA	ADA+TADA
Dataset1	0.3441	0.3575	0.4078	0.4594	0.3485	0.3739	0.3436	0.5027
Dataset2	0.4606	0.4213	0.5202	<u>0.5206</u>	0.5357	0.4419	0.4479	0.4869
Dataset3	<u>0.6170</u>	0.6009	0.5728	0.5668	0.5960	0.5774	0.6252	0.5802
Dataset4	0.6164	0.6023	0.5888	0.5663	0.5873	0.5680	0.5898	0.5822
Dataset5	0.6706	0.6777	0.6118	<u>0.6711</u>	0.6530	0.6639	0.6550	0.6576
Average	0.5417	0.5319	0.5405	<u>0.5568</u>	0.5441	0.5250	0.5323	0.5619

4.3 Performance Evaluation in combining the variants of ADA with TADA

One advantage of our proposed method is its compatibility with existing adversarial data augmentation techniques. We have integrated techniques from extensions of ADA, such as M-ADA [32] and ME-ADA [2], into TADA, resulting in variants like ME-TADA and M-TADA. As shown in Tables 1, 2, and 3, TADA can be effectively combined with ADA, leading to the development of combinations such as ME-(ADA+TADA) and M-(ADA+TADA).

Table 4 presents the average F1 scores for each domain dataset. The results suggest that merging ADA with TADA generally enhances performance across datasets. Specifically, ADA+TADA yields the highest F1 score in the Physionet dataset, demonstrating the advantages of this combination. In the PCL dataset, M-(ADA+TADA) provides a significant performance improvement. Additionally, in the HHAR dataset, M-TADA outperforms other combinations. These findings indicate that applying TADA to relax worst-case scenarios is more effective than adopting a maximum-entropy criterion. This underscores the importance of tailoring the combination of data augmentation techniques to the unique characteristics of each dataset for optimal performance.

Table 4: Average F1 score of the variants of ADA with TADA for all datasets

	TADA	ME-TADA	M-TADA	ADA+TADA	ME-(ADA+TADA)	M-(ADA+TADA)
Physionet	0.4625	0.4542	<u>0.4650</u>	0.4708	0.4645	0.4598
PCL	0.6114	0.6203	0.6191	<u>0.6214</u>	0.6211	0.6735
HHAR	0.5323	0.5492	0.5878	<u>0.5619</u>	0.5429	0.5268

4.4 Visualization of Distribution Shifts

We claim that TADA induces a different type of distribution shift (e.g., a distribution with temporally shifted samples) compared to the distribution shift caused by ADA (e.g., a distribution with amplitude-modified samples). We expect that these two distinct distributions could effectively enhance the robustness and generalization of models for time series data. For verification purposes, we first extract samples from both the training dataset (i.e., a single source sub-dataset) and the test dataset (i.e., other target sub-datasets). We then employ UMAP [33] to visualize their scatteredness.

Figure 1 displays the UMAP visualization for the datasets. Gray dots represent original samples from the target sub-datasets, which are likely the data points that the model aims to generalize towards. Orange dots represent samples from the source sub-dataset; these are the original data points on which the model may have been initially trained. Blue dots represent samples that have been augmented using ADA, which include amplitude variations of the source data. Green dots are samples generated by TADA, focusing on temporal shifts not covered by ADA.

The visualization reveals that gray and orange dots are somewhat intermixed but also form distinct clusters, indicating some overlap yet distinguishable characteristics between the source and target datasets. The blue and green dots are interspersed among the original source and target samples. The placement of these augmented points suggests that they bridge the gap between the characteristics of the source and target datasets, potentially aiding in improving model generalization by providing a gradient of features between these datasets.

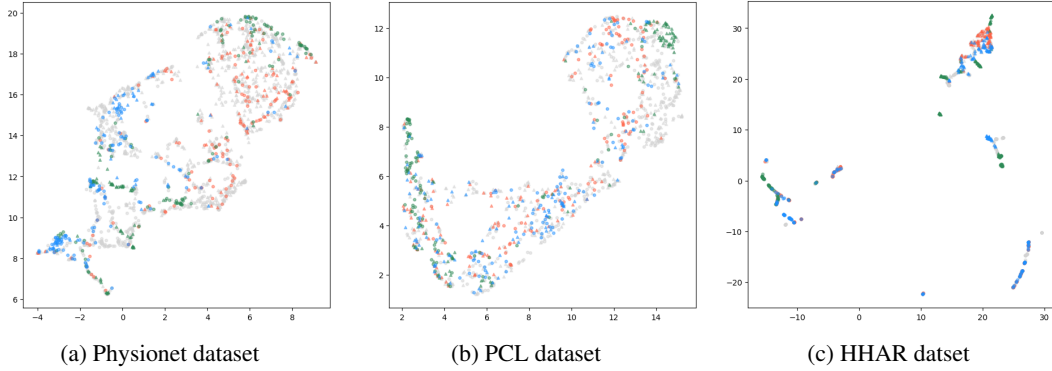


Figure 1: UMAP visualization for datasets.

5 Conclusion

We introduce the Adversarial Data Augmentation for time series data (TADA) as a novel approach to address domain generalization challenges specific to time series data. TADA effectively supplements traditional Adversarial Data Augmentation (ADA), which has predominantly focused on amplitude-related distribution shifts but often overlooks temporal aspects crucial to time series analysis. By leveraging a differentiable time-warping technique that utilizes the duality between time warping in the time domain and phase shifts in the frequency domain, TADA is capable of addressing the temporal distribution shifts that ADA misses. Our extensive evaluations across diverse datasets such as electrocardiograms, electroencephalograms, and human activity recordings demonstrate that TADA not only outperforms existing ADA variants but also accurately simulates real-world data shifts. The integration of TADA and ADA provides a comprehensive solution that significantly enhances model robustness and generalization capabilities across unseen domains. Our findings suggest that

TADA can be seamlessly integrated into existing ADA frameworks, improving their effectiveness and allowing them to better simulate and adapt to real-world distribution shifts. Ultimately, TADA represents a significant advancement in overcoming the challenges posed by distribution shifts in time series data, thereby enhancing the practical applicability and robustness of machine learning models in real-world scenarios.

References

- [1] Riccardo Volpi, Hongseok Namkoong, Ozan Sener, John C Duchi, Vittorio Murino, and Silvio Savarese, “Generalizing to unseen domains via adversarial data augmentation,” *Advances in neural information processing systems*, vol. 31, 2018.
- [2] Long Zhao, Ting Liu, Xi Peng, and Dimitris Metaxas, “Maximum-entropy adversarial data augmentation for improved generalization and robustness,” *Advances in Neural Information Processing Systems*, vol. 33, pp. 14435–14447, 2020.
- [3] Kaiyang Zhou, Ziwei Liu, Yu Qiao, Tao Xiang, and Chen Change Loy, “Domain generalization: A survey,” *arXiv e-prints*, pp. arXiv–2103, 2021.
- [4] Krikamol Muandet, David Balduzzi, and Bernhard Schölkopf, “Domain generalization via invariant feature representation,” in *International Conference on Machine Learning*. PMLR, 2013, pp. 10–18.
- [5] Haoliang Li, Sinno Jialin Pan, Shiqi Wang, and Alex C Kot, “Domain generalization with adversarial feature learning,” in *Proceedings of the IEEE conference on computer vision and pattern recognition*, 2018, pp. 5400–5409.
- [6] Christopher Chatfield, *The analysis of time series: theory and practice*, Springer, 2013.
- [7] Robert H Shumway, David S Stoffer, and David S Stoffer, *Time series analysis and its applications*, vol. 3, Springer, 2000.
- [8] Meinard Müller, “Dynamic time warping,” *Information retrieval for music and motion*, pp. 69–84, 2007.
- [9] Xinyu Yang, Zhenguo Zhang, Xu Cui, and Rongyi Cui, “A time series data augmentation method based on dynamic time warping,” in *2021 International Conference on Computer Communication and Artificial Intelligence (CCAI)*. IEEE, 2021, pp. 116–120.
- [10] Matthew A Reyna, Nadi Sadr, EA Perez Alday, Annie Gu, Amit Shah, Chad Robichaux, AB Rab, Andoni Elola, Salman Seyedi, Sardar Ansari, et al., “Will two do? varying dimensions in electrocardiography: The physionet/computing in cardiology challenge 2021,” *Computing in Cardiology*, vol. 48, pp. 1–4, 2021.
- [11] Jean-Christophe Gagnon-Audet, Kartik Ahuja, Mohammad-Javad Darvishi-Bayazi, Pooneh Mousavi, Guillaume Dumas, and Irina Rish, “Woods: Benchmarks for out-of-distribution generalization in time series,” *arXiv preprint arXiv:2203.09978*, 2022.
- [12] Zijian Wang, Yadan Luo, Ruihong Qiu, Zi Huang, and Mahsa Baktashmotlagh, “Learning to diversify for single domain generalization,” in *Proceedings of the IEEE/CVF International Conference on Computer Vision*, 2021, pp. 834–843.
- [13] Benjamin Recht, Rebecca Roelofs, Ludwig Schmidt, and Vaishal Shankar, “Do imagenet classifiers generalize to imagenet?,” in *International conference on machine learning*. PMLR, 2019, pp. 5389–5400.
- [14] Jose G Moreno-Torres, Troy Raeder, Rocío Alaiz-Rodríguez, Nitesh V Chawla, and Francisco Herrera, “A unifying view on dataset shift in classification,” *Pattern recognition*, vol. 45, no. 1, pp. 521–530, 2012.
- [15] Rohan Taori, Achal Dave, Vaishal Shankar, Nicholas Carlini, Benjamin Recht, and Ludwig Schmidt, “Measuring robustness to natural distribution shifts in image classification,” *Advances in Neural Information Processing Systems*, vol. 33, pp. 18583–18599, 2020.
- [16] Gilles Blanchard, Gyemin Lee, and Clayton Scott, “Generalizing from several related classification tasks to a new unlabeled sample,” *Advances in neural information processing systems*, vol. 24, 2011.
- [17] Yang Shu, Zhangjie Cao, Chenyu Wang, Jianmin Wang, and Mingsheng Long, “Open domain generalization with domain-augmented meta-learning,” in *Proceedings of the IEEE/CVF conference on computer vision and pattern recognition*, 2021, pp. 9624–9633.

- [18] Kaiyang Zhou, Ziwei Liu, Yu Qiao, Tao Xiang, and Chen Change Loy, “Domain generalization: A survey,” *IEEE Transactions on Pattern Analysis and Machine Intelligence*, 2022.
- [19] Ziqi Wang, Marco Loog, and Jan Van Gemert, “Respecting domain relations: Hypothesis invariance for domain generalization,” in *2020 25th International Conference on Pattern Recognition (ICPR)*. IEEE, 2021, pp. 9756–9763.
- [20] Brecht Laperre, Jorge Amaya, and Giovanni Lapenta, “Dynamic time warping as a new evaluation for dst forecast with machine learning,” *Frontiers in Astronomy and Space Sciences*, p. 39, 2020.
- [21] Patrick Wagner, Nils Strodthoff, Ralf-Dieter Bousseljot, Dieter Kreiseler, Fatima I Lunze, Wojciech Samek, and Tobias Schaeffter, “Ptb-xl, a large publicly available electrocardiography dataset,” *Scientific Data*, vol. 7, no. 1, pp. 1–15, 2020.
- [22] Jianwei Zheng, Jianming Zhang, Sidy Danioko, Hai Yao, Hangyuan Guo, and Cyril Rakovski, “A 12-lead electrocardiogram database for arrhythmia research covering more than 10,000 patients,” *Scientific data*, vol. 7, no. 1, pp. 1–8, 2020.
- [23] Jianwei Zheng, Huimin Chu, Daniele Struppa, Jianming Zhang, Magdi Yacoub, Hesham El-Askary, Anthony Chang, Louis Ehwerhemuepha, Islam Abudayyeh, Alexander Barrett, et al., “Optimal multi-stage arrhythmia classification approach,” *Scientific reports*, vol. 10, no. 1, pp. 1–17, 2020.
- [24] Feifei Liu, Chengyu Liu, Lina Zhao, Xiangyu Zhang, Xiaoling Wu, Xiaoyan Xu, Yulin Liu, Caiyun Ma, Shoushui Wei, Zhiqiang He, et al., “An open access database for evaluating the algorithms of electrocardiogram rhythm and morphology abnormality detection,” *Journal of Medical Imaging and Health Informatics*, vol. 8, no. 7, pp. 1368–1373, 2018.
- [25] Pang Wei Koh, Shiori Sagawa, Henrik Marklund, Sang Michael Xie, Marvin Zhang, Akshay Balsubramani, Weihua Hu, Michihiro Yasunaga, Richard Lanus Phillips, Irena Gao, et al., “Wilds: A benchmark of in-the-wild distribution shifts,” in *International conference on machine learning*. PMLR, 2021, pp. 5637–5664.
- [26] Diederik P Kingma and Jimmy Ba, “Adam: A method for stochastic optimization,” *arXiv preprint arXiv:1412.6980*, 2014.
- [27] Leslie N Smith and Nicholay Topin, “Super-convergence: Very fast training of neural networks using large learning rates,” in *Artificial intelligence and machine learning for multi-domain operations applications*. SPIE, 2019, vol. 11006, pp. 369–386.
- [28] Liam Li, Kevin Jamieson, Afshin Rostamizadeh, Ekaterina Gonina, Moritz Hardt, Benjamin Recht, and Ameet Talwalkar, “Massively parallel hyperparameter tuning,” *arXiv preprint arXiv:1810.05934*, vol. 5, 2018.
- [29] Philipp Moritz, Robert Nishihara, Stephanie Wang, Alexey Tumanov, Richard Liaw, Eric Liang, Melih Elibol, Zongheng Yang, William Paul, Michael I Jordan, et al., “Ray: A distributed framework for emerging {AI} applications,” in *13th {USENIX} Symposium on Operating Systems Design and Implementation ({OSDI} 18)*, 2018, pp. 561–577.
- [30] Hongyi Zhang, Moustapha Cisse, Yann N Dauphin, and David Lopez-Paz, “Mixup: Beyond empirical risk minimization,” *arXiv preprint arXiv:1710.09412*, 2017.
- [31] Zhenlin Xu, Deyi Liu, Junlin Yang, Colin Raffel, and Marc Niethammer, “Robust and generalizable visual representation learning via random convolutions,” *arXiv preprint arXiv:2007.13003*, 2020.
- [32] Fengchun Qiao, Long Zhao, and Xi Peng, “Learning to learn single domain generalization,” in *Proceedings of the IEEE/CVF conference on computer vision and pattern recognition*, 2020, pp. 12556–12565.
- [33] Leland McInnes, John Healy, and James Melville, “Umap: Uniform manifold approximation and projection for dimension reduction,” *arXiv preprint arXiv:1802.03426*, 2018.

Appendix

A Visualizing Samples Generated through Adversarial Data Augmentation

The figures in this section display samples generated by ADA and TADA. As shown in the figure, ADA perturbs the samples by adjusting their amplitude, whereas TADA their temporal characteristics. This confirms that TADA perturbs time series data as intended.

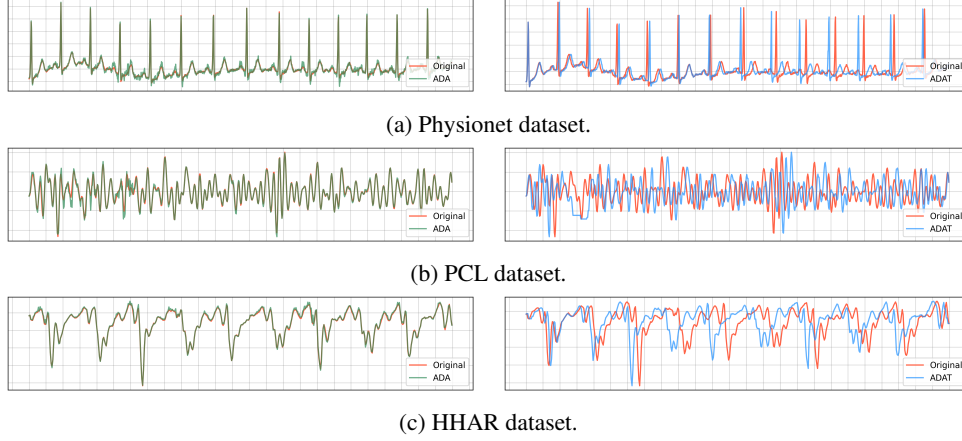


Figure 2: Examples of adversarially generated samples in three datasets.

B Algorithm for ADA+TADA

During the data generation phase (the inner maximization phase), we can add samples generated from both ADA and TADA to the dataset, instead of relying solely on samples generated from either method. TADA can be implemented in conjunction with ADA by iteratively applying both methods during the data generation phase, as detailed in lines 10-18 of Algorithm 2.

Algorithm 2 ADA+TADA

```

1: Input: original dataset  $\{X_i, Y_i\}_{i=1}^n$  and initialized weights  $\theta_0$ 
2: Output: learned weights  $\theta$ 
3: Initialize:  $\theta \leftarrow \theta_0$ 
4: for  $k = 1, \dots, K$  do
5:   for  $t = 1, \dots, T_{min}$  do
6:     Sample  $(X_t, Y_t)$  uniformly from dataset
7:      $\theta \leftarrow \theta - \alpha \nabla_{\theta} \mathcal{L}(\theta; X_t, Y_t)$ 
8:   end for
9:   Sample  $\{X_i, Y_i\}_{i=1}^n$  uniformly from the dataset
10:  for  $F = F^{ADA}, F^{TADA}$  do
11:    for  $i = 1, \dots, n$  do
12:      Initialize:  $\phi_i^k \leftarrow \phi_0$ 
13:      for  $t = 1, \dots, T_{max}$  do
14:         $\phi_i^k \leftarrow \phi_i^k + \eta \nabla_{\phi} \{\mathcal{L}(\theta; (F(X_i, \phi_i^k), Y_i)) - \gamma c_{\phi}((F(X_i, \phi_i^k), Y_i), (X_i, Y_i))\}$ 
15:      end for
16:      Append  $(F(X_i, \phi_i^k), Y_i)$  to dataset
17:    end for
18:  end for
19: end for
20: for  $t = 1, \dots, T$  do
21:   Sample  $(X, Y)$  uniformly from dataset
22:    $\theta \leftarrow \theta - \alpha \nabla_{\theta} \mathcal{L}(\theta; (X, Y))$ 
23: end for

```

C Additional Experimental Result

The tables in this section present detailed experimental results for Physionet, PCL, and HHAR datasets. Each table reports the performance of various approach based on on the source and target domain. The average results for the target domains are summarized in Tables 1, 2, and 3, which are used to evaluate the performance of each approach in section 4.2.

Table 5: F1 score on the Physionet dataset

Source	Target	ERM	Mixup	RandConv	ADA	ME-ADA	M-ADA	TADA	ADA+TADA
PTBXL	G12EC	0.5633	0.5449	0.5538	0.5403	0.5457	0.5256	0.5652	0.5586
PTBXL	CPSC2018	0.3521	0.3402	0.3462	0.3246	0.3335	0.3311	0.3643	0.3576
PTBXL	Chapman	0.5304	0.5302	0.5294	0.5069	0.5215	0.5255	0.5400	0.5419
PTBXL	Ningbo	0.5313	0.5518	0.5157	0.5005	0.5331	0.4773	0.5132	0.5245
PTBXL	Average	0.4943	0.4918	0.4863	0.4681	0.4834	0.4649	0.4957	0.4956
G12EC	PTBXL	0.4062	0.3977	0.3840	0.3971	0.4012	0.3998	0.4108	0.4077
G12EC	CPSC2018	0.3520	0.3526	0.3420	0.3392	0.3367	0.3464	0.3568	0.3506
G12EC	Chapman	0.5307	0.5539	0.5408	0.5401	0.5330	0.5551	0.5481	0.5480
G12EC	Ningbo	0.5622	0.5850	0.5768	0.5759	0.5604	0.5850	0.5824	0.5820
G12EC	Average	0.4628	0.4723	0.4609	0.4631	0.4578	0.4716	0.4745	0.4721
CPSC2018	PTBXL	0.2927	0.3084	0.2910	0.2795	0.3242	0.2873	0.2933	0.2826
CPSC2018	G12EC	0.4143	0.4340	0.4278	0.3912	0.4134	0.3890	0.3866	0.4027
CPSC2018	Chapman	0.4089	0.4376	0.4299	0.4224	0.3979	0.4108	0.3888	0.4117
CPSC2018	Ningbo	0.4121	0.4084	0.4266	0.4066	0.3653	0.3866	0.3573	0.3979
CPSC2018	Average	0.3820	0.3971	0.3938	0.3749	0.3752	0.3684	0.3565	0.3737
Chapman	PTBXL	0.4119	0.4070	0.4150	0.3991	0.4340	0.4099	0.4236	0.4231
Chapman	G12EC	0.5136	0.5143	0.5322	0.4868	0.5296	0.5152	0.5127	0.5321
Chapman	CPSC2018	0.3119	0.3107	0.3247	0.2868	0.3221	0.2843	0.3030	0.3129
Chapman	Ningbo	0.5869	0.5896	0.6090	0.5980	0.5911	0.5978	0.5958	0.6268
Chapman	Average	0.4561	0.4554	0.4702	0.4427	0.4692	0.4518	0.4588	0.4737
Ningbo	PTBXL	0.4826	0.4885	0.4953	0.4845	0.4802	0.4840	0.4913	0.4923
Ningbo	G12EC	0.5901	0.5967	0.6134	0.5758	0.5937	0.5873	0.5951	0.6047
Ningbo	CPSC2018	0.3373	0.3665	0.3690	0.3464	0.3639	0.3417	0.3587	0.3727
Ningbo	Chapman	0.6595	0.6767	0.6620	0.6527	0.6725	0.6620	0.6635	0.6857
Ningbo	Average	0.5174	0.5321	0.5349	0.5149	0.5276	0.5188	0.5272	0.5389

Table 6: F1 score on the PCL dataset

Source	Target	ERM	Mixup	RandConv	ADA	ME-ADA	M-ADA	TADA	ADA+TADA
Dataset1	Dataset2	0.6642	0.6548	0.7015	0.6675	0.6552	0.6333	0.6710	0.6444
Dataset1	Dataset3	0.6092	0.6060	0.5815	0.6060	0.5977	0.4592	0.6142	0.5962
Dataset1	Average	0.6367	0.6304	0.6415	0.6368	0.6264	0.5463	0.6426	0.6203
Dataset2	Dataset1	0.5832	0.5748	0.5864	0.6094	0.5741	0.5367	0.5640	0.5796
Dataset2	Dataset2	0.6327	0.6131	0.6255	0.6222	0.6158	0.5871	0.6348	0.6526
Dataset2	Average	0.6079	0.5939	0.6060	0.6158	0.5949	0.5619	0.5994	0.6161
Dataset3	Dataset1	0.5328	0.5556	0.4730	0.5420	0.5406	0.4500	0.5388	0.5782
Dataset3	Dataset2	0.6467	0.6446	0.6271	0.6450	0.6383	0.5907	0.6458	0.6771
Dataset3	Average	0.5897	0.6001	0.5501	0.5935	0.5895	0.5204	0.5923	0.6277

Table 7: F1 score on the HHAR dataset

Source	Target	ERM	Mixup	RandConv	ADA	ME-ADA	M-ADA	TADA	ADA+TADA
Dataset1	Dataset2	0.6459	0.7101	0.7362	0.7242	0.6923	0.5995	0.6267	0.6950
Dataset1	Dataset3	0.2444	0.2400	0.2790	0.3868	0.2367	0.2398	0.2440	0.4344
Dataset1	Dataset4	0.1956	0.2297	0.2729	0.3691	0.2305	0.2364	0.2260	0.4382
Dataset1	Dataset5	0.2906	0.2501	0.3430	0.3576	0.2345	0.2301	0.2778	0.4431
Dataset1	Average	0.3441	0.3574	0.4078	0.4594	0.3485	0.3265	0.3436	0.5027
Dataset2	Dataset1	0.6530	0.6852	0.6583	0.6948	0.7241	0.6595	0.6406	0.7247
Dataset2	Dataset3	0.4012	0.3364	0.4733	0.4601	0.4514	0.4789	0.3900	0.4081
Dataset2	Dataset4	0.3993	0.3197	0.4434	0.4443	0.4764	0.4781	0.3612	0.4143
Dataset2	Dataset5	0.3887	0.3439	0.5056	0.4831	0.4908	0.4952	0.3999	0.4004
Dataset2	Average	0.4606	0.4213	0.5202	0.5206	0.5357	0.5279	0.4479	0.4869
Dataset3	Dataset1	0.2334	0.2029	0.1347	0.1227	0.2407	0.1652	0.2884	0.1771
Dataset3	Dataset2	0.3576	0.3422	0.3015	0.2958	0.3134	0.3026	0.3719	0.2822
Dataset3	Dataset4	0.9984	0.9955	0.9972	0.9978	0.9985	0.9978	0.9954	0.9979
Dataset3	Dataset5	0.8786	0.8628	0.8617	0.8508	0.8313	0.8553	0.8449	0.8636
Dataset3	Average	0.6170	0.6008	0.5738	0.5668	0.5960	0.5802	0.6251	0.5802
Dataset4	Dataset1	0.2433	0.2087	0.1601	0.1483	0.1396	0.1638	0.1710	0.1811
Dataset4	Dataset2	0.3770	0.3481	0.3264	0.2651	0.3412	0.2743	0.3197	0.2974
Dataset4	Dataset3	0.9995	0.9995	0.9973	0.9987	0.9990	0.9995	0.9988	0.9966
Dataset4	Dataset5	0.8458	0.8527	0.8715	0.8532	0.8692	0.8298	0.8698	0.8537
Dataset4	Average	0.6164	0.6022	0.5888	0.5663	0.5873	0.5669	0.5898	0.5822
Dataset5	Dataset1	0.3237	0.3090	0.1913	0.2817	0.2387	0.2606	0.2555	0.2762
Dataset5	Dataset2	0.4145	0.4439	0.3318	0.4184	0.4303	0.3292	0.3907	0.3971
Dataset5	Dataset3	0.9726	0.9791	0.9638	0.9923	0.9724	0.9901	0.9876	0.9779
Dataset5	Dataset4	0.9714	0.9788	0.9602	0.9920	0.9890	0.9704	0.9861	0.9790
Dataset5	Average	0.6705	0.6777	0.6118	0.6711	0.6530	0.6422	0.6550	0.6575

D Additional Visualization of Distribution Shift

Figure 3 display the detailed distribution of representations previously introduced on Figure 1 in Section 4.4 . Each row in Figure 1 (a), (b), and (c) corresponds to a different class. As discussed in section 4.4, there are notable distribution difference between the source and unseen datasets. Both ADA and TADA address these discrepancies, with each method covering distinct regions.

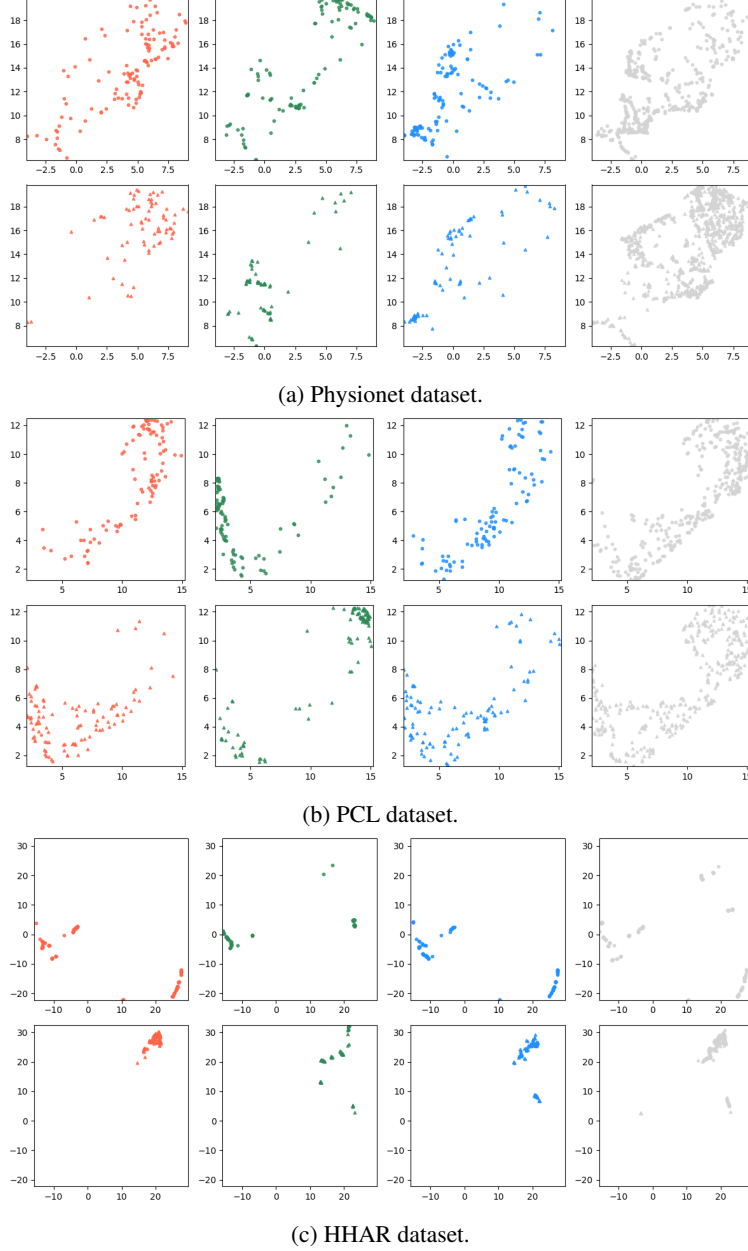


Figure 3: Examples of adversarially generated samples in three datasets.